Data Assimilation for Fault Slip Monitoring and Short-Term Prediction of Slow Slip Events: Application to the 2010 Long-Term Slow Slip Event in the Bungo Channel, Japan

Masayuki Kano[1,2] (ORCID: 0000-0002-7288-4760),

Yusuke Tanaka[1] (ORCID: 0000-0003-4907-4919),

Daisuke Sato[2] (ORCID: 0000-0001-8809-9268),

Takeshi Iinuma[2] (ORCID: 0000-0003-0386-2055), and

Takane Hori[2] (ORCID: 0000-0003-3769-3894)

MK: Conceptualization, Methodology, Formal analysis, Funding acquisition, Writing—original draft, review & editing

YT: Data curation, Writing—review & editing

DS: Supervision, Writing—review & editing

TI: Supervision, Writing—review & editing

TH: Supervision, Writing—review & editing

[1]Graduate School of Science, Tohoku University, Sendai, Japan.

[2]Japan Agency for Marine-Earth Science and Technology, Yokohama, Japan.

Corresponding author: M. Kano (masayuki.kano.a3@tohoku.ac.jp)

Key Points:

- We developed a data assimilation (DA) method for fault slip monitoring and short-term prediction of slow slip events (SSEs)
- Crustal deformation observed during the 2010 Bungo Channel SSE was quantitatively reproduced through DA
- Observations of slow nucleation were not enough to predict evolution to an SSE or earthquake without prior information on slip style

Abstract

Monitoring and predicting fault slip behaviors in subduction zones are essential for understanding earthquake cycles and assessing future earthquake potential. We developed a data assimilation (DA) method for fault slip monitoring and short-term prediction of slow slip events (SSEs), which was applied to the 2010 Bungo Channel SSE in southwest Japan. The observed geodetic data were quantitatively explained using a physics-based model with DA. We investigated short-term predictability by assimilating observation data with limited periods. Without prior constraint on fault slip style, observations solely during slip acceleration predicted the occurrence of a fast slip; however, the inclusion of slip deceleration data successfully predicted a slow transient slip. With prior constraint to exclude unstable slip, the assimilation of data after the SSE occurrence predicted a slow transient slip. This study provided a tool using DA for fault slip monitoring and prediction based on real observation data.

Plain Language Summary

Various fault slips ranging from fast dynamic rupture to slow steady motion have been observed in subduction zones. Understanding the current slip and predicting how it will evolve in the near future are essential for assessing future slip behavior including earthquakes. Data assimilation (DA) combines physics-based models and observations and is widely used in weather forecasting. We developed a DA method for monitoring and predicting the fault slip of slow slip events (SSEs) and applied it to real observations for the first time. The target SSE was the 2010 Bungo Channel SSE in southwest Japan, where SSEs were observed at recurrence intervals of approximately six to seven years. We demonstrated that DA can reproduce observed crustal deformation during the SSE. Additionally, we examined short-

52 term predictability by assuming a scenario in which we acquire data for an ongoing SSE.
53 Without the knowledge of the fault slip style, the observations of slow fault acceleration were
54 not enough to predict whether it will evolve to a slow transient slip or fast dynamic rupture;
55 therefore, the accumulation of data helped in constraining the possible scenarios for future
56 slip evolution. Our study provides a basis for monitoring fault slips and their short-term
57 prediction using DA.
58

59 **Keywords**
60 Slow slip event, Data assimilation, Global Navigation Satellite System, Bungo Channel,
61 Frictional parameter
62

1 Introduction

Monitoring fault slip behaviors in subduction zones and predicting their short-term evolution are critical for understanding seismic cycles. Specifically, we define the term "monitoring" as estimating the spatio-temporal evolution of fault slips based on various observation data and "prediction" as using physics-based numerical simulations to assess how current slip behaviors might evolve in the imminent future through. One direct approach to address both tasks is to employ data assimilation (DA) techniques (e.g., Fletcher, 2022; Lewis et al., 2006). DA combines observation data with numerical models to obtain a more realistic model that quantitatively explains the observations. DA is widely used in meteorology and oceanology, particularly in practical applications such as weather forecasting.

DA have been adopted for fault slip estimations in plate subduction zones (Fukuda et al., 2009; Kano et al., 2020; van Dinther et al., 2019). Most previous studies have focused on the optimization problem of frictional properties, which determine the fault slip behavior in the physics-based model, and/or the initial values of simulation variables such as slip velocities on the fault. Through optimization, observation data were quantitatively explained by physics-based models. Various DA methods have been applied to the fault slip problem, including the Markov chain Monte Carlo (MCMC) method (Fukuda et al., 2009), particle filter (Hori et al., 2014; Mitsui et al., 2010), ensemble Kalman filter (EnKF) (Diab-Montero et al., 2023; Hirahara & Nishikiori, 2019; van Dinther et al., 2019) and adjoint method (Kano et al. 2013). Most of these previous studies have validated their proposed method through numerical experiments using synthetic observations, with only a few studies utilizing real observations.

DA employing real observations was successfully applied to the afterslip that followed the 2003 magnitude 8.0 Tokachi-oki earthquake that occurred off the Tokachi

region, northeast Japan. Fukuda et al. (2009) applied the MCMC method to successfully estimate the posterior probability density functions (PDFs) of frictional parameters, using a single spring-slider system with a sub-daily Global Navigation Satellite System (GNSS) time series for 5 h following the mainshock. Kano et al. (2015, 2020) developed the adjoint DA method to optimize spatially variable frictional parameters and/or initial slip velocities from daily GNSS data for 15 days following the mainshock and examined the short-term predictability of afterslip for another 15 days by comparing the misfit between the observed and numerically predicted crustal deformations.

Slow slip events (SSEs) are another research target of DA (Diab-Montero et al., 2023; Hirahara & Nishikiori, 2019). Many observational studies have inferred that SSEs occurred prior to megathrust earthquakes (e.g., Ito et al., 2013; Radiguet et al., 2016; Ruiz et al., 2014; Voss et al., 2018), and therefore, monitoring and predicting the spatio-temporal evolution of SSEs are important, particularly for assessing future earthquake potential. Hirahara and Nishikiori (2019) (hereafter referred as HN19) first introduced DA to the fault slip estimation problem of SSEs focusing on long-term SSEs in the Bungo Channel, southwest Japan. Through numerical experiments, they demonstrated that the EnKF successfully estimated frictional parameters on the fault where the SSE occurred.

In contrast to previous studies, to our knowledge, the present study is the first to apply DA to real observations of SSEs. Assuming the fault model in HN19, we assimilate GNSS data recorded during the 2010 Bungo Channel SSE using the MCMC method. Although this fault model is relatively simple, we focus on how such a simple model could explain the GNSS observations and predict their short-term temporal evolutions. An attempt is also made to predict the temporal evolution during a single SSE, which assumes the situation that an SSE is currently ongoing. We aim to evaluate the short-term evolution of fault slip. This

corresponds to short-term prediction of SSEs with timescales ranging from weeks to at most a few years.

In the remainder of this paper, we first briefly describe the DA settings. We then present the monitoring and prediction results for the 2010 Bungo Channel SSE. Finally, we discuss the predictability of the SSE's short-term evolution. Through this analysis, the present study proposes a strategy for realtime fault slip monitoring and prediction using DA.

2 Settings of DA

2.1. Physics-based model in the Bungo Channel long-term SSE

The Bungo Channel is located southwest of Japan in the Nankai subduction zone, where the Philippine Sea Plate subducts beneath the Amurian Plate (Figure 1a). Beneath the Bungo Channel, SSEs with a moment magnitude of ~7 were repeatedly observed around 1980, 1985, 1991, 1997, 2003, 2010, and 2018 based on geodetic observations (Hirose et al., 1999; Kobayashi & Yamamoto 2011; Ozawa et al., 2013; Seshimo & Yoshioka 2022; Yoshioka et al., 2015). HN19 introduced a fault model that mimicked these observed characteristics of the SSEs (Figure 1a). The fault model represents a subducting plate interface as a single rectangular fault with a dip angle of 15° extending to 120 km × 100 km in the strike and dip directions, respectively. The entire fault is divided into subfaults with sizes of 2 km × 2 km; thus, the total number of subfaults is 3000. Each subfault was assumed to obey the following quasi-dynamic equation of motion (Rice, 1993):

$$\tau_i(t) = \sum_j k_{ij}(v_{\mathrm{pl}}t - s_j(t)) - \frac{G}{2\beta}v_i(t), \tag{1}$$

where the slip velocity $v_i(t)$, shear stress $\tau_i(t)$, and slip $s_i(t)$ (=d$v_i(t)$/dt) are the temporally changing simulation variables at subfault i. The second term on the right side of Equation (1)

represents the radiation damping (Rice, 1993) accounting for energy release owing to seismic wave radiation rather than the inertial term. The slip response function k_{ij} represents a change in shear stress at subfault i due to a unit slip at subfault j and is calculated assuming a linear isotropic elastic homogeneous half-space (Okada, 1992). The plate velocity v_{pl}, shear modulus G, and shear wave velocity β are set as 6.5 cm/yr (Miyazaki & Heki 2001), 40 GPa, and 3.0 km/s, respectively.

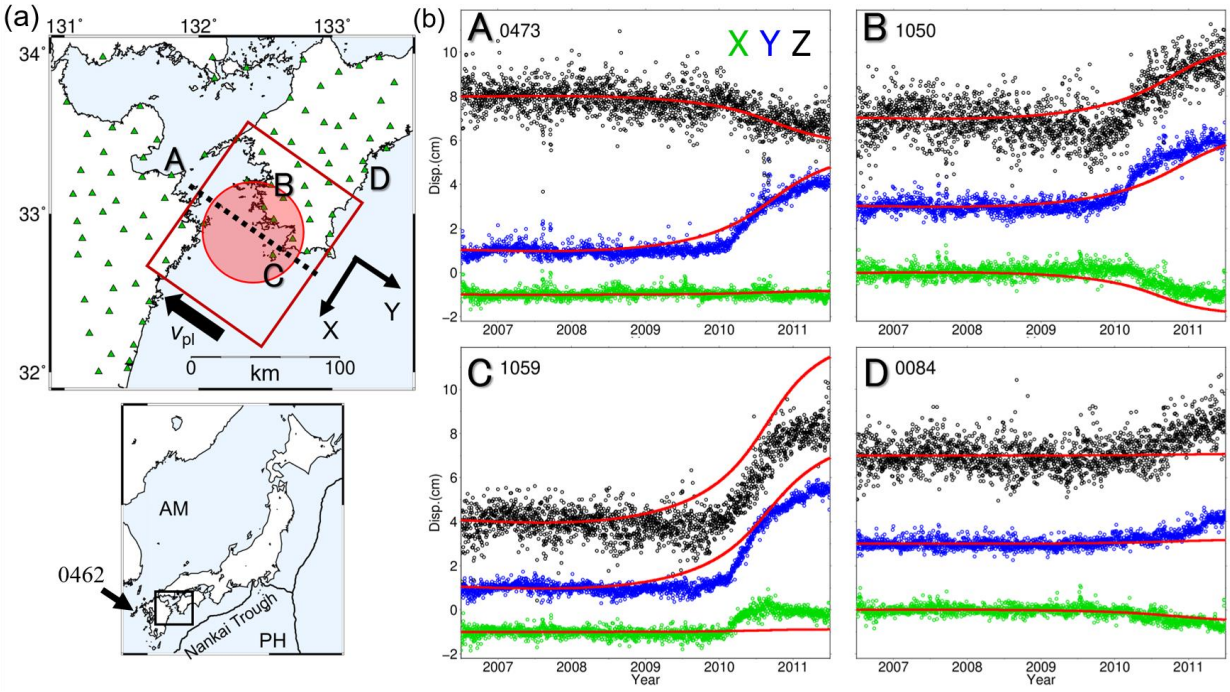

Figure 1. (a: top panel) The study area in southwest Japan is marked by the black rectangle in the lower image. The red square represents the Bungo Channel SSE fault region assumed by Hirahara & Nishikiori (2019). This study assumes uniform frictional parameters both inside and outside the SSE patch indicated in the red circle. The locations of GNSS stations are marked by green rectangles, with the time series for stations A–D presented in (b). The temporal slip evolution, denoted by the dotted line, is shown in Figure S2. (a: bottom panel) The tectonic setting of the study area, in which the Philippine Sea Plate (PH) subducts beneath the Amurian Plate (AM) along the Nankai Trough. (b) Examples of GNSS time

series at stations identified in (a). The displacements in trench-parallel (X), trench-perpendicular (Y), and vertical (Z) components are represented by green, blue, and black dots, respectively. The red lines depict the calculated time series, derived from 100 frictional parameters sampled from the posterior PDF of the model parameters. Note that red lines largely overlap, making it visually difficult to distinguish the 100 time series in each component.

To express the slip behavior of SSEs, HN19 set a circular patch of SSE with a radius of R = 35 km, whose center corresponds to the center of the entire fault at a depth of 25 km. HN19 used the rate- and state-dependent friction law with the aging state evolution law described by Equations (2) and (3) (Dieterich, 1979; Ruina, 1983):

$$\tau_i(t) = \tau_{0i} + A_i \ln\left(\frac{v_i(t)}{v_0}\right) + B_i \ln\left(\frac{v_0\theta_i(t)}{L_i}\right), \tag{2}$$

$$\frac{\mathrm{d}\theta_i(t)}{\mathrm{d}t} = 1 - \frac{v_i(t)\theta_i(t)}{L_i}, \tag{3}$$

where $\theta_i(t)$ is a state variable representing the state of the sliding surface. τ_0 is the reference shear stress corresponding to shear stress τ for steady sliding at a reference velocity v_0; however, these reference values were not explicitly set here because we only calculate shear stress rate. The frictional parameters A_i, B_i, and L_i that characterize the fault slip behavior at subfault i were assumed to be uniform inside and outside the circular patch. HN19 set the frictional parameters as (A-B, A, and L) = (-50 kPa, 100 kPa, and 40 mm) and (70 kPa, 100 kPa, and 40 mm) for subfaults inside and outside the SSE patch, respectively. These frictional parameters were determined based on the critical nucleation size R_c:

$$R_c = \frac{\pi}{3}\frac{GBL}{(B-A)^2}. \tag{4}$$

For an isolated patch, when $R/R_c << 1$, the calculated fault slip becomes stable, while an unstable slip occurs when $R/R_c > 1$ for $0.5 < A/B < 1$ (Chen & Lapsuta, 2009; Hirahara & Nishikiori, 2019). HN19 set the frictional parameters corresponding to $R/R_c \sim 0.35$, such that the calculated slip behavior was similar to that of the long-term SSEs. The following calculations focus only frictional parameters inside the patch; parameters outside the patch were set to be the same as HN19 throughout the study.

Combining Equations (1)–(3), the temporal evolution of slip velocity $v_i(t)$ can be expressed as follows:

$$\frac{dv_i(t)}{dt} = \frac{\sum_j k_{ij}(v_{\mathrm{pl}} - v_j(t)) - \frac{B_i}{\theta_i(t)}\left(1 - \frac{v_i(t)\theta_i(t)}{L_i}\right)}{\frac{A_i}{v_i} + \frac{G}{2\beta}}. \quad (5)$$

By setting the initial conditions, we numerically solved Equations (3) and (5) to obtain the temporal evolutions of two independent simulation variables $v_i(t)$ and $\theta_i(t)$ for each subfault using the fourth-order embedded Runge–Kutta method (Press et al., 1996). Consequently, HN19 successfully reproduced the observed characteristics such as recurrence intervals, durations, and maximum slip velocity, in the long-term SSE of the Bungo Channel. Hereafter, we focus on one cycle of the long-term SSE, and define the initial time as two years prior to the SSE initiation when $\mathrm{d}\theta/\mathrm{d}t$ was approximately zero. We fixed the initial values of simulation variables at this initial time throughout the study.

2.2. GNSS observations

This study focuses on the Bungo Channel SSE that occurred from 2009 to 2011. Crustal deformations due to the SSE were monitored by the GNSS Earth Observation

Network System (GEONET) operated by the Geospatial Information Authority of Japan. We used the daily GNSS time series from 86 GEONET stations around the Bungo Channel that were used in HN19 after removing seven stations that were unavailable during the analysis period (Figure 1a). The data period is from January 2006 to December 2011. The original time series were preprocessed using the GipsyX-1.4 software (Bertiger et al., 2020) under the precise point processing strategy with ambiguity resolution analysis. Station 0462 (Fukue) was used as a reference site (Figure 1a). After preprocessing, we corrected offsets resulting from antenna replacement and large earthquakes by subtracting the differences between the coordinates respectively averaged for 10 days before and after the offset. We then rotated the two horizontal components to the trench-parallel (X-axis) and trench-perpendicular (Y-axis) components and subtracted the inter-SSE effect by fitting a linear function to the time series from 2006.5 to 2008.5. The standard deviation for each time series was calculated from the residuals of this linear trend fitting. Finally, we visually checked each time series to determine whether they included any ambiguous change; if so, the station was not used in the subsequent analysis.

Figure 1b shows examples of the GNSS time series, indicating that the transient signal initiated in mid-2009 and continued for approximately two years. In the following analysis, we first assimilated the GNSS time series of the three components between 2008.5 and 2011.5 for fault slip monitoring. Subsequently, to test the predictability of the short-term evolution of fault slips, we changed the data period used for DA (hereafter referred to as the DA period) to 0.5, 1.0, 1.5, 2.0, and 2.5 years. In these trials, the initial time of the DA period was fixed to 2008.5, while the end was set to be 2009.0, 2009.5, 2010.0, 2010.5, or 2011.0, respectively.

2.3. MCMC method

In this study, DA is conducted using MCMC, which is a technique to obtain a realization or sample **m** from a target probability density function (PDF) $p(\mathbf{m})$. In our problem, the target PDF is the posterior PDF of the model parameter $p(\mathbf{m}|\mathbf{d})$, where **m** consists of a set of three frictional parameters (A, B, and L) within the SSE patch, and **d** is the observation vector. Therefore, we aimed not only to optimize the frictional parameters but also to evaluate their uncertainties. Using this information, the temporal evolution of fault slip can be predicted in a probabilistic manner.

Among the wide variety of MCMC methods, we used the Metropolis method, which is one of the well-known versatile algorithms (Metropolis et al., 1953). The posterior PDF is calculated using Bayes' theorem $p(\mathbf{m}|\mathbf{d}) = cp(\mathbf{m})p(\mathbf{d}|\mathbf{m})$, where $p(\mathbf{m})$ is a prior PDF of the model parameters, $p(\mathbf{d}|\mathbf{m})$ is a likelihood function, and c is a constant that is canceled out in the Metropolis method. We assume two types of prior information: uniform distributions for all the frictional parameters, and those with constraints of $R/R_c < 0.58$, that is, $R_c > 60$ km, and $0.5 < A/B < 1$. The latter prior PDF is introduced to avoid unstable slip and assumes that we know SSE will occur in the target area. The likelihood function $p(\mathbf{d}|\mathbf{m})$ is defined as the product of the misfits between the calculated and observed crustal deformations, scaled by the observation errors with a normalization constant c':

$$p(\mathbf{d}\,|\,\mathbf{m}) = c' \prod_{t=1}^{N} \exp\left(-\frac{1}{2} (\mathbf{H}\mathbf{s}_t - \mathbf{d}_t)^{\mathrm{T}} \mathbf{R}^{-1} (\mathbf{H}\mathbf{s}_t - \mathbf{d}_t) \right), \tag{6}$$

where $\mathbf{d}_t$ includes the observed cumulative displacement on day t. $\mathbf{s}_t$ contains the fault slip for all subfaults, and **H** is an observation matrix that converts simulation variables, or fault slip in this case, to observed quantities. Therefore, the product $\mathbf{H}\mathbf{s}_t$ corresponds to the calculated cumulative displacement. In this study, the observation matrix **H** was calculated by assuming

a linear isotropic elastic homogeneous half-space (Okada, 1992). $\mathbf{R}_t$ includes the observation errors described in the previous subsection, and N is the number of observation epochs.

The Metropolis method iteratively obtains the samples $\mathbf{m}$ from the posterior PDF $p(\mathbf{m}|\mathbf{d})$ using the initial values of $\mathbf{m}^0 = (A, B, L)^{\mathrm{T}} = (100\ \mathrm{kPa}, 150\ \mathrm{kPa}, 40\ \mathrm{mm})^{\mathrm{T}}$, which are used in HN19.

For $k = 0, 1, \ldots, K\text{-}1$, repeat the following steps.

1. Propose a candidate for the next sample $\mathbf{m}$' based on the following proposal distribution and the current sample $\mathbf{m}^k$:

$$\mathbf{m}' = \boldsymbol{\xi}, \quad \boldsymbol{\xi} \sim N\left(\mathbf{m}^k, \boldsymbol{\Sigma}\right). \tag{7}$$

We assume $\boldsymbol{\Sigma}$ is a diagonal matrix.

2. Determine whether the candidate $\mathbf{m}$' is accepted or not with an acceptance ratio of $min(1, p(\mathbf{m}'|\mathbf{d})/p(\mathbf{m}^k|\mathbf{d}))$. If the candidate is accepted, we set $\mathbf{m}^{k+1} = \mathbf{m}'$; otherwise, $\mathbf{m}^{k+1} = \mathbf{m}^k$.

We do not use the initial samples to remove the effect of the initial values. After this initial burn-in period, the resulting series of samples $\{\mathbf{m}^k\}$ ($k = 0, 1, \ldots, K$) emulates an objective sample set drawn from a target posterior PDF $p(\mathbf{m}|\mathbf{d})$.

For each iteration, we ran a forward simulation with the initial simulation variables and assigned frictional parameters to obtain the calculated crustal deformation, which was then detrended using the time series for the first two years. Subsequently, we compared the calculated displacement with the observations to obtain a sample. We first repeated these procedures for K = 10,000 iterations for the global parameter search with a standard deviation of 5.0×10^{-1} kPa, 1.0 kPa, and 1.0×10^{-1} mm for A-B, A, and L, respectively in diagonal components of Σ. Following this, we conducted an additional 10,000 iterations with values of 5.0×10^{-3} kPa, 1.0×10^{-2} kPa, and 1.0×10^{-3} mm for A-B, A, and L, respectively, for the local

search and obtained samples of the posterior PDF of the model parameters from the latter 10,000 samples.

3 Fault Sip Monitoring Results of the 2010 Bungo SSE

This section presents the results obtained by assimilating the GNSS data, including the entire SSE period from 2008.5 to 2011.5. Frictional parameters within the SSE patch were estimated as A-B = -43.1 kPa, A = 77.5 kPa, and L = 45.9 mm (Table 1 and Figure S1). The uncertainty of each parameter was approximately five orders of magnitude smaller than the parameter value itself. This implies that a slight change in the parameters will greatly decrease the posterior PDF values, and the proposed values will rarely be accepted in the MCMC. This may be due to the strong constraint of the assumed simple numerical fault model, in which the location of the SSE patch is fixed, the frictional parameters are assumed to be spatially uniform within the patch, and the slip direction is fixed. Future studies should consider applying the method to a numerical model with a high degrees-of-freedom, considering the spatial heterogeneity in frictional parameters, variable slip directions, and geometry of the subducting plate interface.

Despite this model constraint, the calculated displacement time series using 100 randomly selected samples in Figure S1 explained the observed GNSS data (Figure 1b). Notably, all 100 calculated time series mostly overlap; thus, Figure 1b indicates the small uncertainty of the calculated displacement, reflecting the small uncertainty of the parameters. Fault slips along the plate interface slowly accelerated in 2009 and lasted for ~2 years with a maximum slip rate of $\log(V/V_{pl})$~0.55 (~11 cm/yr) (Figure S2). These characteristics are roughly consistent with the kinematic inversion results of Yoshioka et al. (2015), demonstrating the reproducibility of the observed crustal deformation by DA.

4 Short-Term Prediction of Slip Evolutions of Ongoing SSE

We next investigated the short-term predictability of ongoing SSE by changing the DA period. This setting assumes that if we observe the currently ongoing transient signal, we can predict its future evolution over subsequent days to months based on the estimated frictional parameters by DA. Figures 2a, 2b and Table 1 summarize the DA and prediction results and the estimated frictional parameters. Figures 2a and 2b indicate that all results successfully explained the observed data during the DA period. However, the prediction results showed different behaviors depending on the DA period: when we assimilated data for a DA period of 2.5 years (orange line), the future evolution was predicted as a slow transient slip. However, when we assimilated data for DA periods shorter than 2.0 years (green, blue, and purple lines), the prediction resulted in a fast slip (Figure 2b). This implies that without prior knowledge of observations showing the deceleration of a fault slip, or in other words, when we only have observations during slip acceleration, the results predict the occurrence of an earthquake. The estimated frictional parameters in the case of short DA periods correspond to unstable slip conditions of $R/R_c > 1$ (Table 1).

Following these results, we conducted similar DA trials with a prior constraint on the critical nucleation size R_c to avoid unstable slip. The resulting time series calculated using the estimated frictional parameters (Table 1) predicted slow transient slip rather than unstable slip (green, blue, and purple lines in Figure 3c). For cases with a DA period longer than 2.5 years, the proposed samples in the MCMC computation are not rejected by the prior constraints, and therefore, the results matched those without a prior constraint on R_c.

311

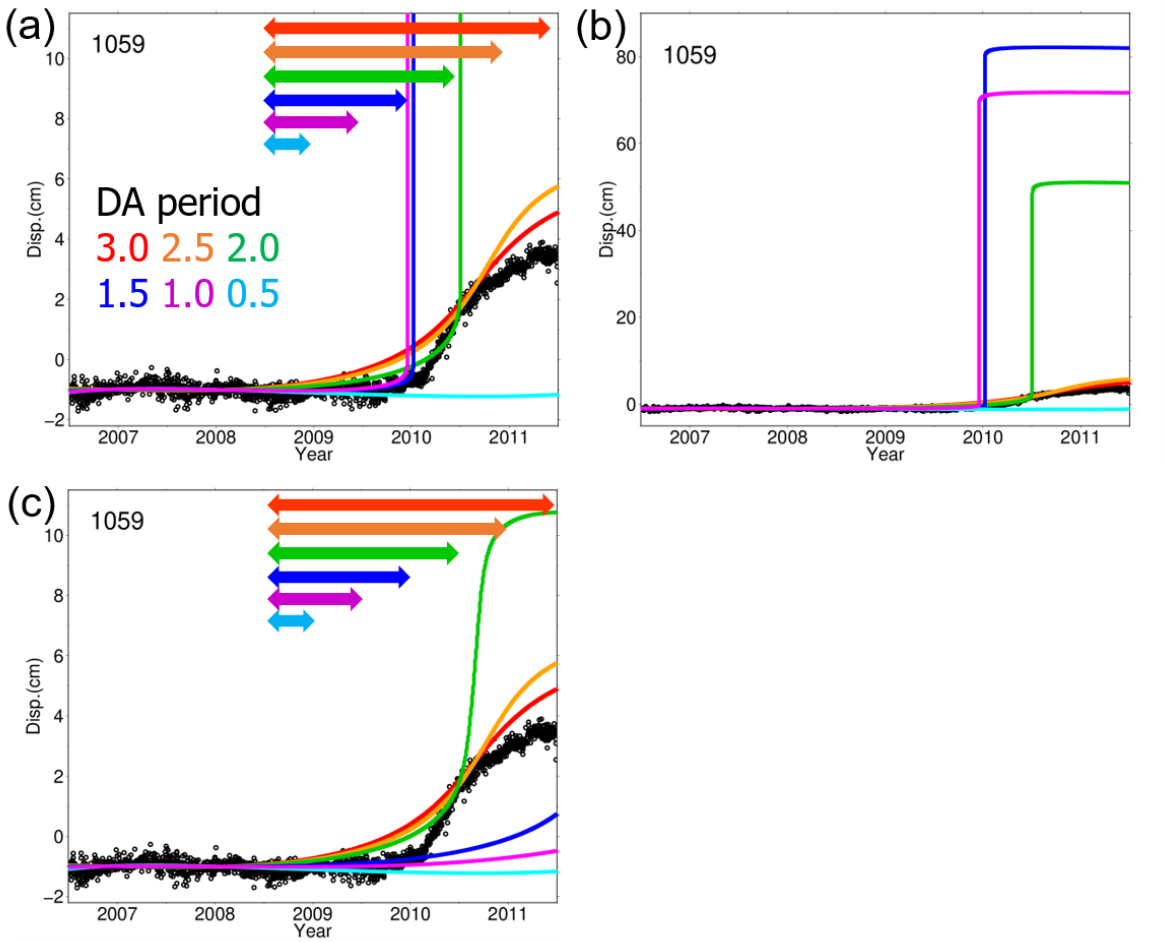

312

313 **Figure 2**. (a) Comparison of observed (circles) and calculated (colored lines) time series
314 without prior constraints on the critical nucleation size R_c in the trench-perpendicular
315 component at station 1059. The calculated time series are computed using 100 frictional
316 parameters sampled from the posterior PDF of the model parameters by assimilating the
317 observations indicated by the corresponding colored arrows. Notably, the colored lines
318 largely overlap, making it visually difficult to distinguish the 100 calculated time series. (b)
319 An enlarged view of (a) in the vertical axis. (c) Same as (a) but with prior constraints on R_c.

320

Table 1. *Estimated frictional parameters and their uncertainties (s.d.) without and with prior constraints on critical nucleation size R_c.*

DA period	A-B (kPa) (s.d.)	A (kPa) (s.d.)	L (mm) (s.d.)	R_c (km)
Without prior constraints on critical nucleation size R_c				
0.5 yrs	-191.7 (3.2)	30.7 (4.1)	69.3 (1.1)	17.6
1.0 yr	-161.5 (8.7×10^{-2})	19.3 (1.7×10^{-1})	55.2 (8.5×10^{-3})	16.1
1.5 yrs	-180.7 (6.1×10^{-2})	39.3 (1.6×10^{-1})	46.1 (1.5×10^{-2})	13.1
2.0 yrs	-116.7 (9.4×10^{-4})	125.2 (8.9×10^{-4})	39.3 (7.7×10^{-5})	29.2
2.5 yrs*	-57.3 (3.9×10^{-4})	67.4 (4.3×10^{-4})	51.6 (1.8×10^{-4})	82.1
3.0 yrs*	-43.1 (3.1×10^{-4})	77.5 (3.8×10^{-4})	45.9 (1.3×10^{-4})	124.6
**	-50.0	100	40.0	100
With prior constraints on critical nucleation size R_c				
0.5 yrs	-137.8 (3.6)	355.6 ($1.3\times10^{+1}$)	71.8 (2.3)	78.2
1.0 yr	-78.2 (5.8×10^{-2})	78.3 (1.4×10^{-1})	86.0 (1.2×10^{-2})	92.2
1.5 yrs	-82.1 (4.1×10^{-2})	86.7 (1.2×10^{-1})	57.4 (1.2×10^{-2})	60.2
2.0 yrs	-71.3 (7.5×10^{-4})	105.6 (4.4×10^{-4})	41.1 (5.1×10^{-5})	60.0
2.5 yrs*	-57.3 (3.9×10^{-4})	67.4 (4.3×10^{-4})	51.6 (1.8×10^{-4})	82.1
3.0 yrs*	-43.1 (3.1×10^{-4})	77.5 (3.8×10^{-4})	45.9 (1.3×10^{-4})	124.6
**	-50.0	100	40.0	100

Note. * Same values for both results with and without prior constraints

**Values used in Hirahara & Nishikiori (2019).

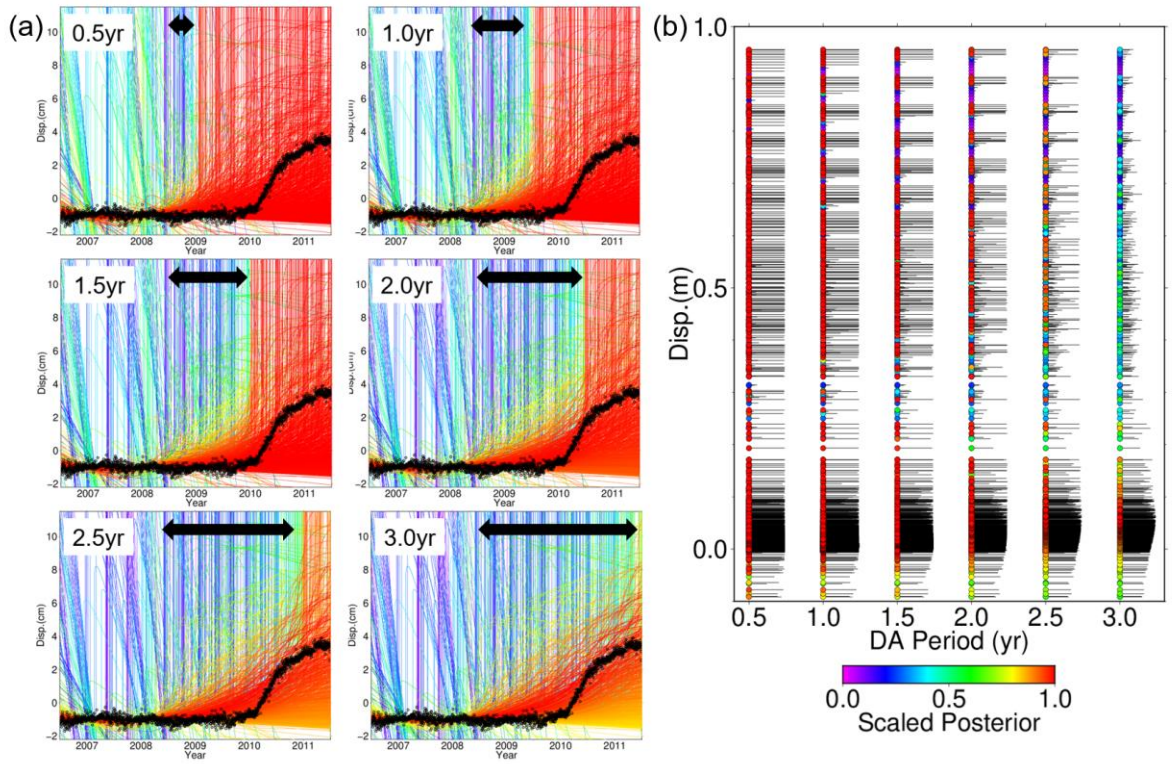

Figure 3. (a) Comparison of observed (black circles) and calculated (colored lines) time series, in the trench-perpendicular component at station 1059. These calculated time series are derived by varying a set of frictional parameters. The line colors correspond to posterior values calculated using the data in the DA period indicated by the black arrow in each subpanel. These posterior values are scaled to a range [0,1] within each subpanel. (b) Scaled posterior values as functions of the DA period in the horizontal axis and final displacement in 2011.5 shown in (a) in the vertical axis. The length of each horizontal black line corresponds to the scaled posterior values.

Regardless of the prior constraint on R_c, the uncertainties in the frictional parameters decreased with increasing number of observation epochs (Table 1). This implies that the number of possible scenarios for future slip evolution decreased with data accumulation. To clarify this point, we analyzed possible scenarios for future slip evolution based on forward computations by varying the frictional parameters. We set a combination of frictional

343 parameters A-B = -210.0–30.0 kPa, A = 10.0–150.0 kPa, and L = 30.0–100.0 mm with
344 increments of A-B = 10.0 kPa, A = 10.0 kPa, and L = 10.0 mm. Thus, we conducted 1,862
345 forward computations, excluding the sets of frictional parameters with which numerical
346 integration could not be executed owing to strongly unstable behavior. In each computation,
347 the posterior values were evaluated for all DA periods. Figure 3a summarizes all calculated
348 time series or scenarios in each DA period in the Y-direction at station 1059. For trials with
349 short DA periods, the time series with high posterior PDF predicted both fast and slow slips
350 after the DA period. With long DA period, only few time series tended to predict fast slips
351 (i.e., a reduction in the number of vertical red lines), and scenarios for predicting SSEs were
352 dominant. This characteristic can be clearly observed in Figure 3b, which shows scaled
353 posterior values as functions of the DA period on the horizontal axis and the final
354 displacement in 2011.5 shown in Figure 3a. This final displacement approximately
355 corresponded to the mode of the calculated fault slips; the final displacement was large (> a
356 few tens of cm) for fast slip, moderate (~ a few to 10 cm) for slow slip, and small (~0 cm) for
357 stable slip. The scaled posterior values indicate that almost all the slip scenarios are possible
358 for a DA period of 0.5 years. When the DA periods became longer, the scenarios with fast
359 slips were gradually rejected. Finally, those with high scaled posterior values favor a slow
360 fault slip of ~6 cm in final displacement at station 1059, particularly in cases with DA periods
361 longer than 2.5 years.

362 This study assumed uniform distribution of frictional parameters as a prior PDF.
363 Bayesian estimation enables the sequential update of the prior PDF, and the posterior PDF
364 was eventually obtained after DA (Figure 3b and Table 1). The posterior PDF can be utilized
365 as prior information when conducting DA for the next SSE.

366 In summary, the observed GNSS time series were quantitatively explained by the DA,
367 independent of the DA period, even when using the simplified fault model proposed by

HN19. For short-term prediction, information on the deceleration of slip velocities is necessary to appropriately constrain the evolution of the SSE; otherwise, the DA predicts fast fault slips. Although a high degree of freedom would result in better fault slip monitoring and short-term prediction with high accuracy, the present results demonstrate the effectiveness of the DA for monitoring and predicting the evolution of SSEs.

Acknowledgments

This study was supported by the MEXT Project for Seismology toward Research Innovation with Data of Earthquake (STAR-E) (Grant number JPJ010217), ERI JURP 2022-B-06 in Earthquake Research Institute, the University of Tokyo, and JSPS KAKENHI (Grant numbers JP21K03694, JP21H05206, and JP23H00466). The computer system in Earthquake Research Institute, the University of Tokyo, was used in this study.

Data Availability Statement

The original GNSS data from GEONET used in this study can be downloaded from https://www.gsi.go.jp/ENGLISH/geonet_english.html after registration. Figures were generated using Generic Mapping Tools (Wessel et al., 2013).

References

Bertiger, W., Bar-Sever, Y., Dorsey, A., Haines, B., Harvey, N., Hemberger, D., et al. (2020). GipsyX/RTGx, a new tool set for space geodetic operations and research. *Advances in Space Research*, *66*(3), 469–489. https://doi.org/10.1016/j.asr.2020.04.015

Chen, T., & Lapusta, N. (2009). Scaling of small repeating earthquakes explained by interaction of seismic and aseismic slip in a rate and state fault model. *Journal of Geophysical Research: Solid Earth, 114*(B1). https://doi.org/10.1029/2008JB005749

Diab-Montero, H. A., Li, M., van Dinther, Y., & Vossepoel, F. C. (2023). Estimating the occurrence of slow slip events and earthquakes with an ensemble Kalman filter. *Geophysical Journal International*, *234*(3), 1701–1721. https://doi.org/10.1093/gji/ggad154

Dieterich, J. H. (1979). Modeling of rock friction: 1. Experimental results and constitutive equations. *Journal of Geophysical Research: Solid Earth*, *84*(B5), 2161–2168. https://doi.org/10.1029/JB084iB05p02161

Fletcher, S. J. (2022). Data assimilation for the geosciences: From theory to application. Elsevier.

Fukuda, J., Johnson, K. M., Larson, K. M., & Miyazaki, S. (2009). Fault friction parameters inferred from the early stages of afterslip following the 2003 Tokachi-oki earthquake. *Journal of Geophysical Research: Solid Earth*, *114*(B4). https://doi.org/10.1029/2008JB006166

Hirahara, K., & Nishikiori, K. (2019). Estimation of frictional properties and slip evolution on a long-term slow slip event fault with the ensemble Kalman filter: numerical experiments. *Geophysical Journal International*, *219*(3), 2074–2096. https://doi.org/10.1093/gji/ggz415

Hirose, H., Hirahara, K., Kimata, F., Fujii, N., & Miyazaki, S. (1999). A slow thrust slip event following the two 1996 Hyuganada earthquakes beneath the Bungo Channel, southwest Japan. *Geophysical Research Letters*, *26*(21), 3237–3240. https://doi.org/10.1029/1999GL010999

Hori, T., Miyazaki, S. I., Hyodo, M., Nakata, R., & Kaneda, Y. (2014). Earthquake forecasting system based on sequential data assimilation of slip on the plate boundary. *Theoretical and Applied Mechanics Japan*, *62*, 179–189. https://doi.org/10.11345/nctam.62.179.

Ito, Y., Hino, R., Kido, M., Fujimoto, H., Osada, Y., Inazu, D., et al. (2013). Episodic slow slip events in the Japan subduction zone before the 2011 Tohoku-Oki earthquake. *Tectonophysics*, *600*, 14–26. https://doi.org/10.1016/j.tecto.2012.08.022

Kano, M., Miyazaki, S., Ito, K., & Hirahara, K. (2013). An adjoint data assimilation method for optimizing frictional parameters on the afterslip area. *Earth, Planets and Space*, *65*, 1575–1580. https://doi.org/10.5047/eps.2013.08.002

Kano, M., Miyazaki, S., Ishikawa, Y., Hiyoshi, Y., Ito, K., & Hirahara, K. (2015). Real data assimilation for optimization of frictional parameters and prediction of afterslip in the 2003 Tokachi-oki earthquake inferred from slip velocity by an adjoint method. *Geophysical Journal International*, *203*(1), 646–663. https://doi.org/10.1093/gji/ggv289

Kano, M., Miyazaki, S., Ishikawa, Y., & Hirahara, K. (2020). Adjoint-based direct data assimilation of GNSS time series for optimizing frictional parameters and predicting postseismic deformation following the 2003 Tokachi-oki earthquake. *Earth, Planets and Space*, *72*(1), 1–24. https://doi.org/10.1186/s40623-020-01293-0

Kobayashi, A., & Yamamoto, T. (2011). Repetitive long-term slow slip events beneath the Bungo Channel, southwestern Japan, identified from leveling and sea level data from 1979 to 2008. *Journal of Geophysical Research: Solid Earth*, *116*(B4). https://doi.org/10.1029/2010JB007822

Lewis, J. M., Lakshmivarahan, S., & Dhall, S. (2006). Dynamic data assimilation: a least squares approach. Cambridge University Press

Metropolis, N., Rosenbluth, A. W., Rosenbluth, M. N., Teller, A. H., & Teller, E. (1953). Equation of state calculations by fast computing machines. *Journal of Chemical Physics*, *21*(6), 1087–1092. https://doi.org/10.1063/1.1699114

Mitsui, N., Hori, T., Miyazaki, S., & Nakamura, K. (2010). Constraining interplate frictional parameters by using limited terms of synthetic observation data for afterslip: a preliminary test of data assimilation. *Theoretical and Applied Mechanics Japan*, *58*, 113–120. https://doi.org/10.11345/nctam.58.113

Miyazaki, S., & Heki, K. (2001). Crustal velocity field of southwest Japan. *Journal of Geophysical Research*, *106*(B3), 4305–4326. https://doi.org/10.1029/2000JB900312

Okada, Y. (1992). Internal deformation due to shear and tensile faults in a half-space. *Bull. Seismol. Soc. Am.*, *82*, 1018–1040.

Ozawa, S., Yarai, H., Imakiire, T., & Tobita, M. (2013). Spatial and temporal evolution of the long-term slow slip in the Bungo Channel, Japan. *Earth, Planets, and Space*, *65*(2), 67–73. https://doi.org/10.5047/eps.2012.06.009

Press, W. H., Teukolsky, S. A., Vetterling, W. T., & Flannery, B. P. (1996). Numerical recipes in Fortran 90 the art of parallel scientific computing. Cambridge university press.

Radiguet, M., Perfettini, H., Cotte, N. et al. (2016). Triggering of the 2014 M_w7.3 Papanoa earthquake by a slow slip event in Guerrero, Mexico. *Nature Geosciences*, *9*, 829–833. https://doi.org/10.1038/ngeo2817

Rice, J. R. (1993). Spatio-temporal complexity of slip on a fault. *Journal of Geophysical Research: Solid Earth*, *98*(B6), 9885–9907. https://doi.org/10.1029/93JB00191

Ruina, A. (1983). Slip instability and state variable friction laws. *Journal of Geophysical Research*, *88*(B12), 10,359–10,370. https://doi.org/10.1029/JB088iB12p10359

Ruiz, S., Metois, M., Fuenzalida, A., Ruiz, J., Leyton, F., Grandin, R., Vigny, C., Madariaga, R., & Campos, J. (2014). Intense foreshocks and a slow slip event preceded the 2014

463 Iquique M_w 8.1 earthquake. *Science*, *345*, 1165–1169.
464 https://doi.org/10.1126/science.1256074
465 Seshimo, Y., & Yoshioka, S. (2022). Spatiotemporal slip distributions associated with the
466 2018–2019 Bungo Channel long-term slow slip event inverted from GNSS data. *Scientific*
467 *Reports*, *12*(1), 343. https://doi.org/10.1038/s41598-021-03982-6
468 van Dinther, Y., Künsch, H. R., & Fichtner, A. (2019). Ensemble data assimilation for
469 earthquake sequences: Probabilistic estimation and forecasting of fault stresses.
470 *Geophysical Journal International*, *217*(3), 1453–1478.
471 https://doi.org/10.1093/gji/ggz063
472 Voss, N., Dixon, T. H., Liu, Z., Malservisi, R., Protti, M., & Schwartz, S. (2018). Do slow
473 slip events trigger large and great megathrust earthquakes?. *Science advances*, *4*(10),
474 eaat8472. https://doi.org/10.1126/sciadv.aat8472
475 Wessel, P., Smith, W. H., Scharroo, R., Luis, J., & Wobbe, F. (2013). Generic mapping tools:
476 improved version released. *Eos, Transactions American Geophysical Union*, *94*(45), 409–
477 410.
478 Yoshioka, S., Matsuoka, Y., & Ide, S. (2015). Spatiotemporal slip distributions of three long-
479 term slow slip events beneath the Bungo Channel, southwest Japan, inferred from
480 inversion analyses of GPS data. *Geophysical Journal International*, *201*(3), 1437–1455.
481 https://doi.org/10.1093/gji/ggv022